Excitation-dependent recombination and diffusion near an isolated dislocation in GaAs

T. H. Gfroerer,[1] C. M. Crowley,[1] C. M. Read,[1] and M. W. Wanlass[2]
[1]*Davidson College, Davidson, North Carolina 28035, USA*
[2]*National Renewable Energy Laboratory, Golden, Colorado 80401, USA*

(Received 9 December 2011; accepted 27 March 2012; published online 7 May 2012)

In low-magnification, plan-view photoluminescence images of a nominally lattice-matched, undoped GaAs/GaInP heterostructure, we observe a random distribution of isolated dark spots. We attribute the dark spots to crystal dislocations, where nonradiative recombination is augmented by transitions utilizing defect-related energy levels between the conduction and valence bands. We note that, when the laser excitation intensity is reduced, the darkened regions expand. At lower excitation, the density of photogenerated electrons and holes is reduced, and they are more likely to reach the defective region before encountering a partner for radiative recombination. When we model the behavior with a simulation that allows for Laplacian diffusion and defect-related recombination only through mid-bandgap energy levels, we do not obtain good agreement between experimental and simulated images. But if we allow for an arbitrary distribution of defect levels, such that the occupation of the levels and bands can change independently, we have more flexibility for fitting the density-dependent recombination rates. The more sophisticated model produces results that are more consistent with experimental images. © *2012 American Institute of Physics*. [http://dx.doi.org/10.1063/1.4709434]

INTRODUCTION

When defects interrupt the periodic potential of a crystal, the local bandstructure is modified to include additional energy levels that can lie in the gap between the conduction and valence bands. Dislocations are extended crystal defects that result in a high density of these localized states. Under photoexcitation, the additional electronic states provide new pathways for nonradiative recombination, which can deplete the local carrier density. Nearby carriers diffuse into these depleted regions, where they experience a higher rate of defect-related recombination. But the diffusion length, which controls the size of the defect-related depletion region, depends on the photoexcitation intensity. At high injection, the density of electrons and holes is higher, so they encounter each other more frequently. Early encounters augment the probability of radiative recombination, reducing the average lifetime and diffusion distance so the carriers are less likely to reach dislocations.

Diffusion to dislocations, where the recombination rate is higher, reduces the conversion efficiency of photovoltaic devices. Under low illumination, the affected region surrounding dislocations is large and photoexcited carriers in the vicinity of the dislocation are lost to defect-related recombination. With increasing illumination, lateral diffusion becomes less important relative to competing phenomena, including current-generating vertical drift. In this report, we explore how the diffusion to an isolated dislocation depends on photoexcitation and the mechanism of defect-related recombination. We show that our experimental images can only be explained by a recombination model that allows for defect levels distributed across the bandgap. The density of these levels and their depth relative to the conduction and valence band edges are adjusted to control the way band occupation and band-to-band (B-B) recombination change with photoexcitation.

Photoluminescence imaging is a quick, non-destructive method for characterizing substrate and epitaxial layer quality and homogeneity in opto-electronic materials.[1] Spatial fluctuations in photoluminescence intensity indicate that recombination pathways vary with location in the structure. In particular, maps of near-bandgap luminescence can be precisely correlated with dislocation patterns measured via x-ray topography.[2] In addition, epitaxial layers often inherit substrate properties, with photoluminescence intensity patterns that replicate the dislocation network of the underlying substrate.[2] Wafer annealing can have a significant impact on these patterns, especially when spectral selection and temperature are used to distinguish different recombination mechanisms.[3]

Photoluminescence images can also be used to estimate free-carrier diffusion lengths. For example, electroluminescence images have been used to study minority carrier diffusion in thick silicon solar cells.[4,5] In III-V semiconductors, diffusion parameters can be obtained by analyzing the luminescence signal near a highly localized generation source. Examples include using a mask to isolate the luminescence at a specified distance[6] and direct imaging of the two-dimensional luminescence profile.[7] In contrast to these measurements of diffusion away from a high density source, we analyze diffusion toward an isolated defect, which serves as a low density sink. By varying the photoexcitation intensity, we can change the free-carrier diffusion lengths and alter the extent of the region that is depleted by the additional defect-related recombination.

EXPERIMENT

The sample structure for this investigation is an unintentionally doped, nominally lattice-matched GaAs/$Ga_{0.515}In_{0.485}P$ double heterostructure grown on a semi-insulating GaAs substrate. Double heterostructures are useful for this type of measurement because the reduction in surface recombination permits an investigation of more fundamental bulk-like material properties. Deposition rate estimates of layer thicknesses are approximately 2 μm for the GaAs active layer and 0.05 μm for the GaInP confinement layers. The active layer thickness was confirmed by selective etching and measuring the height change with a Dektak profilometer. Additional sample features, including spatially integrated temperature-dependent photoluminescence characteristics, were presented in a previous report.[8]

The experimental setup is shown in Fig. 1. The sample is illuminated with an unfocused 532 nm TEM_{00} laser having a full width at half maximum of 0.18 cm. We take precautions to ensure that the laser profile is unchanged as the laser power is adjusted between 1 mW and 1 W. Photoluminescence images are obtained with a Q-Imaging Rolera XR camera, which has extended infrared sensitivity to 1000 nm. The camera is fitted with a Navitar Zoom 7000 lens, which provides $\sim 1\times$ magnification at a working distance of 13 cm. Hence, image pixels map directly onto detector pixels with dimensions w^2 of 13 μm $\times$ 13 μm. Setting the laser power to 1 W and accounting for reflection losses (15% at windows and 30% at the sample surface), the optical power entering each pixel near the center of the laser spot is approximately 2×10^{-5} W, yielding a generation rate of $r_{gen} = 1.5 \times 10^{23}$ electron-hole pairs $cm^{-3}s^{-1}$.

An RG 610 long-pass filter is used to eliminate scattered laser light. The luminescence signal, which peaks at 870 nm, is calibrated by assuming that defect-related recombination is saturated and the radiative efficiency is nearly 100% under high excitation. In this regime, the ratio of the photoluminescence signal (measured in pixel counts/s) to the excitation intensity levels out and cannot be increased further with higher laser powers.[8] We assign unity efficiency to this ratio and use it to scale the lower excitation measurements where defect-related recombination reduces the radiative contribution.

All measurements were conducted at room temperature ($T \sim 296$ K). We did not control the temperature, but the sample block temperature inside the cryostat was monitored during the experiment. We noted a small increase in temperature after the highest power measurement, but the large beam profile and limited exposure time alleviated excessive localized heating. If significant heating had occurred, the radiative rate would be reduced and the nonradiative Auger rate would be elevated. However, we obtain the highest radiative efficiency at the highest power, so these effects do not make a noticeable contribution. The experimental images of an isolated extended defect are shown in Fig. 2. As the laser excitation intensity is reduced, the radiative efficiency decreases and the recombination-depleted region expands. The size of the feature, with a diameter on the order of 100 μm, is comparable to those observed by Hunter in GaAs, which have been linked with the presence of a single dislocation at the center of the darkened spot.[9]

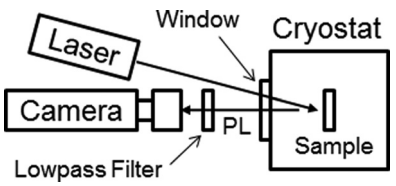

FIG. 1. Experimental setup.

MODELING

We seek to simulate this behavior with a time evolution program that allows for recombination and diffusion-driven flux between adjacent pixels during each time step. Assuming that photogenerated electrons and holes are trapped in deep defect states with similar rates, the density of excess electrons in the conduction band Δn is comparable to the density of excess holes in the valence band Δp, so $\Delta n \approx \Delta p \approx n$ where n is the density of photogenerated electrons or holes. Since the B-B radiative rate r_{rad} is proportional to the product of Δn and Δp, we set $r_{rad} = (B/N)n^2$ $cm^{-3}s^{-1}$, where $B/N \approx 2.2 \times 10^{-11}$ cm^3/s is the radiative coefficient B in GaAs at room temperature divided by the photon recycling factor N.[8] (Our estimate of $N \sim 9$, which accounts for internal reflection and reabsorption of the emitted light, did not assess spectral dependence—we used the mean emission energy in a numerical average over photon trajectories.) In addition, with all defect states located near the middle of the bandgap, we can neglect thermal excitation of trapped carriers back into the bands. Under these conditions, Shockley-Reed-Hall (SRH) recombination through defect levels is proportional to n.[10]

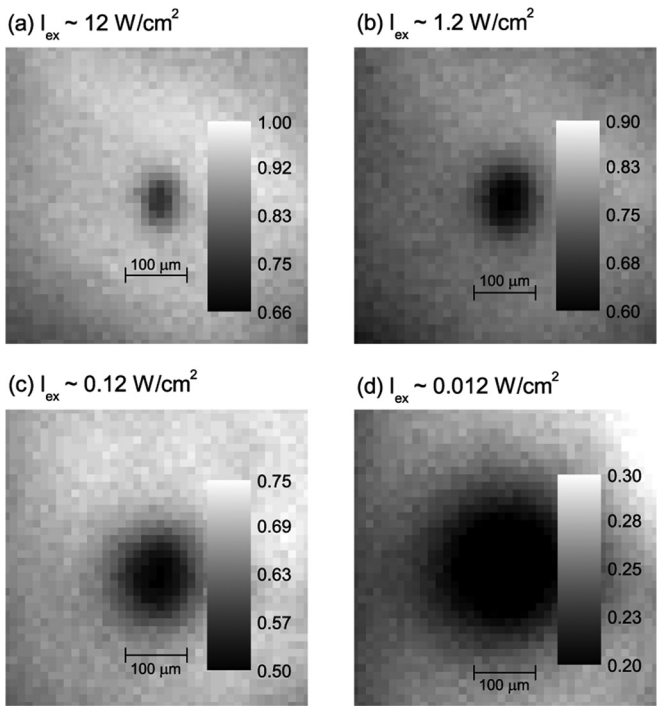

FIG. 2. Experimental plan-view images of the radiative efficiency surrounding an isolated dislocation in the GaAs heterostructure. The temperature $T = 296$ K and the photoexcitation intensity I_{ex} varies as indicated—from 12 W/cm^2 in image (a) to 0.012 W/cm^2 in image (d). Please note the changes in grayscale with changing photoexcitation.

We first model the dislocation as an isolated central pixel with an augmented defect-related recombination rate $r_{def} = A_{dislocation} n$ cm^{-3}s^{-1}. All other pixels share the slower rate $r_{def} = A_{bulk} n$ cm^{-3}s^{-1}, where A_{bulk} accounts for recombination at trace elemental impurities and native point defects like vacancies that are present in all real crystals. We note that the actual augmented rate is not uniform throughout the dislocation pixel but presumably is concentrated to a much smaller unresolved area with dimensions comparable to ordinary extended defects. In each time step, we compute the change in the carrier density n in each pixel via generation, recombination, and Laplacian diffusion into adjacent pixels: $\Delta n = \left(r_{gen} - r_{rad} - r_{def} + D\frac{\partial^2 n}{\partial x^2}\right)\Delta t$, where time steps are limited to ensure that $\Delta n/\Delta t < 10\%$. Here, D is the carrier diffusivity and the second order partial derivative is computed in Cartesian coordinates: $\frac{\partial^2 n}{\partial x^2} = (n_{left} + n_{right} + n_{above} + n_{below} - 4n_{center})/w^2$.

In room temperature GaAs, the electron diffusivity $D_e = 220$ cm^2/s and the hole diffusivity $D_h = 10$ cm^2/s. In our simulations, we have discovered that the hole diffusivity does not provide adequate flux, so D_e is favored in our analysis. Since the laser excitation is relatively uniform throughout the small area under consideration (we estimate that it is only diminished approximately 5% near the edges), we assign the same generation rate to all pixels. The finite element calculation iterates until a steady-state carrier distribution is obtained. Then the simulated and experimental images are compared, and incrementally larger and smaller SRH recombination coefficients are considered. The minimum error (see Fig. 3) is obtained with $A_{dislocation} = 7 \times 10^7$ s^{-1} and $A_{bulk} = 1 \times 10^5$s^{-1}. For this analysis, we manually adjusted the SRH coefficients to obtain images that appeared to match best. Since the variation was readily apparent, we are confident that the given values are accurate to the reported precision. The qualitative agreement between the experimental and simulated images is encouraging, but quantitative agreement is unsatisfactory, particularly at low excitation. If we did not reduce the lower grayscale limit in Fig. 3(d), it would appear even darker.

Upon further analysis, we noted that excellent quantitative agreement could be achieved if we allowed the SRH coefficients to change with excitation. In particular, the simulated images are improved if $A_{dislocation}$ increases systematically as the excitation is reduced, boosting diffusion toward the dislocation. While this exercise is inherently nonphysical because A depends only the density and capture time of the traps (which are constants), the result does point to a more realistic solution. In previous work on this structure, we found that an asymmetric distribution of traps across the bandgap was required to model the excitation-dependent radiative efficiency.[8] With an asymmetric distribution of traps, we get disproportionate occupation of traps and bands. Although this model will require a more sophisticated algorithm, we can expect better results because there are more degrees of freedom. In particular, the new model will allow the B-B and SRH rates to change independently as electrons and holes fill their respective traps: $r_{rad} = (B/N)\Delta p \Delta n$ and $r_{def} = \tau^{-1}(\Delta p \Delta dn + \Delta n \Delta dp)$. In the latter expression, τ is the effective trap capture time and Δdn and Δdp are the densities of trapped electrons and holes, respectively.

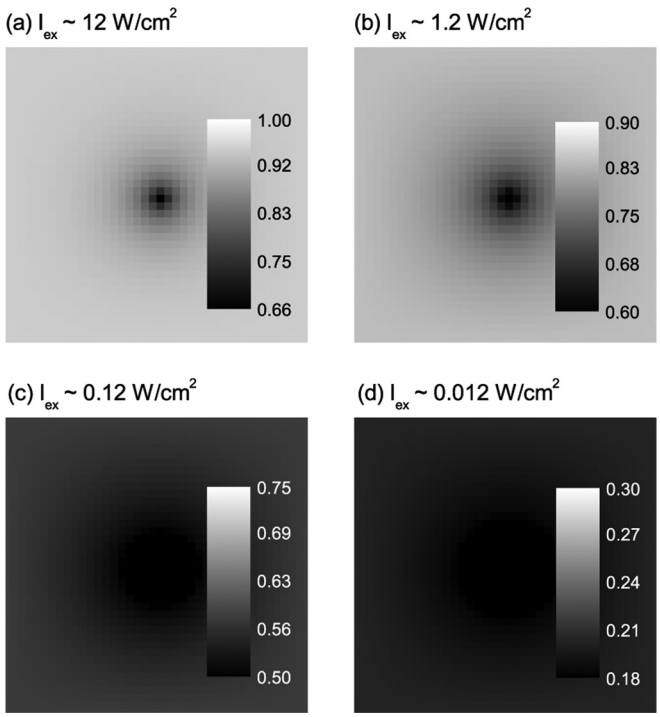

FIG. 3. Simulated plan-view images of the radiative efficiency in room temperature GaAs in the vicinity of an isolated pixel with an elevated SRH recombination coefficient $A_{dislocation} = 7 \times 10^7$ s^{-1}. Image dimensions and grayscales match those used in Fig. 2 with the exception of image (d), where the grayscale lower limit is reduced to reveal the presence of contrast.

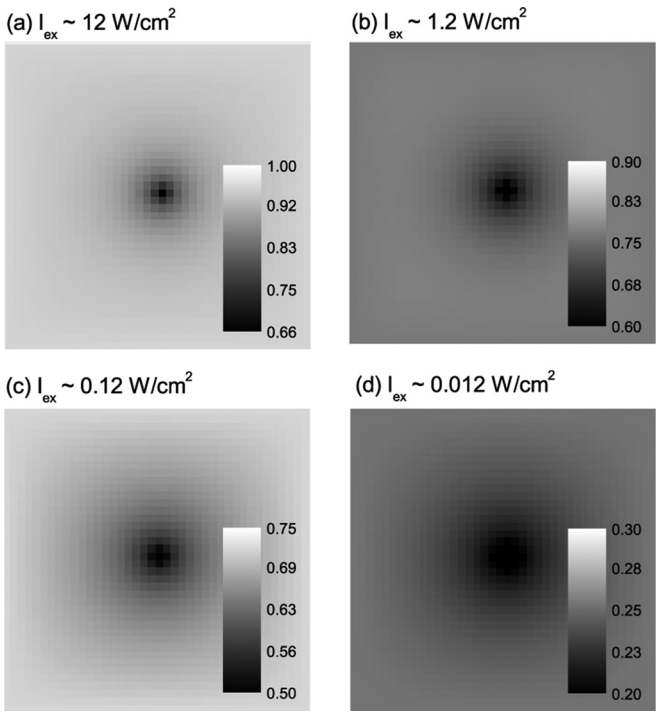

FIG. 4. Simulated plan-view images of the radiative efficiency in GaAs surrounding an isolated pixel with a more concentrated defect-related density of states. DOS functions for the dislocation and bulk pixels are given in Fig. 5. Image dimensions and grayscales are the same as those used in Fig. 2.

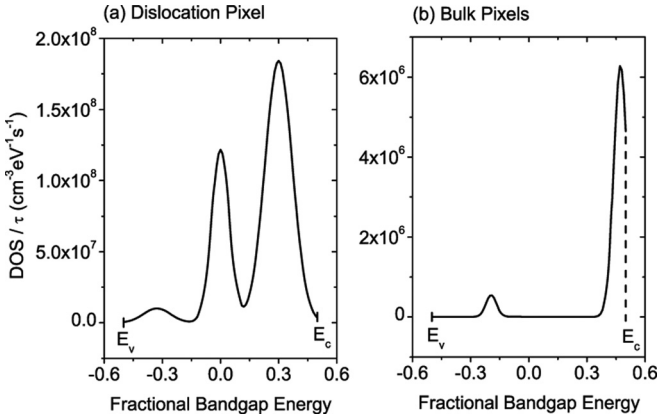

FIG. 5. Computationally generated defect-related DOS functions (between the valence and conduction band edges E_v and E_c) divided by the capture time τ for the dislocation and surrounding bulk pixels. These defect level distributions are used to compute the recombination rates that enter into the diffusion simulations presented in Fig. 4.

Occupation densities and recombination rates depend on the defect-related density of states (DOS) divided by the capture time, which is identified computationally using the algorithm described in Ref. 8. To simplify the analysis, we assume a mid-gap Fermi energy, which should give accurate results for our nominally undoped ($\sim 5 \times 10^{14}$ cm^{-3} n-type) material with the higher injection levels studied here. This recombination model simulates the experimental results quite well (see Fig. 4). The corresponding DOS functions for (a) the central dislocation pixel and (b) the surrounding bulk pixels are shown in Fig. 5. While these functions are not necessarily unique, it is interesting to note that a suitably weighted average of (a) and (b) would produce a DOS similar to the one reported in Ref. 8, which presumably includes spatially weighted contributions from each. Hence, a valuable outcome of this analysis is the ability to distinguish the defect levels associated with extended defects from the levels related to point-like defects in the bulk.

CONCLUSION

As discussed in Ref. 8, the asymmetry of the DOS in the dislocation pixel allows the low excitation SRH recombination rate to grow rapidly while the radiative rate is effectively quenched. Since electrons are trapped disproportionately, few remain in the conduction band for B-B transitions, reducing the radiative efficiency and mimicking the effect of an augmented SRH coefficient $A_{dislocation}$. The defect-related DOS in the surrounding bulk pixels, including a large number of shallow electron traps and fewer but deeper hole traps, may operate as follows. The electron trap peak occurs $\sim$40 meV below the conduction band edge, so many of these states will be thermally depleted at room temperature ($kT \sim 25$ meV). Hence, we would expect the conduction band to sustain occupation as the hole traps fill, once again favoring SRH recombination in the low excitation regime. This scenario corroborates two other important observations that we encountered in our investigation of this structure. First, we found that the radiative efficiency in dislocation-free bulk GaAs was suppressed under low excitation at low temperatures. Freeze-out of electrons in shallow traps would explain this feature. Second, as noted above, we discovered that the electron diffusivity produces superior images in our diffusion simulations. If holes are more likely to be trapped in the dislocation-free region at room temperature, while the dislocation itself retains a high density of deep electron traps, diffusion to the dislocation is more likely to be driven by conduction band electrons. We recognize the possibility of ambipolar effects due to the Coulomb interaction between electrons and holes, but we lack evidence of this phenomenon in our study.

When electron-hole pairs are generated in GaAs-based solar cells, they can recombine by emitting light before being extracted for electricity. Defects in the lattice can provide intermediate energy levels that also allow for heat-generating recombination. Even in high quality solar cells, dislocations produce "dead spots" where defect-related recombination dominates. These extended defects act as sinks, drawing in nearby charge carriers by diffusion. Due to the low population and long lifetime of carriers under low illumination, more distant carriers diffuse to the dislocation, producing a larger dead volume relative to higher illumination conditions. When modeling this phenomenon in GaAs, if we use a simple model that does not account for the occupation of defect and band states separately, we are unable to simulate the experimental images accurately. But if state occupations and recombination rates are computed independently, the model produces images that agree well with experimental results. The above observations have important implications for high-efficiency, III-V-based photovoltaic devices that can operate over a wide range of injection levels.

ACKNOWLEDGMENTS

The authors would like to thank J. J. Carapella for performing the MOVPE growth. Acknowledgment is made to the donors of the American Chemical Society – Petroleum Research Fund for support of this research.

[1]M. Baeumler, C. Fitz, U. Weinberg, J. Wagner, and W. Jantz, Mat. Sci. Eng. B **66**, 131 (1999).
[2]W. Jantz, M. Baeumler, Z. M. Wang, and J. Windscheif, Mat. Res. Soc. Symp. Proc. **325**, 409 (1994).
[3]H. Ch. Alt, M. Neef, and H. von Philipsborn, Appl. Phys. Lett. **55**, 1972 (1989).
[4]T. Fuyuki, H. Kondo, T. Yamazaki, Y. Takahashi, and Y. Uraoka, Appl. Phys. Lett. **86**, 262108 (2005).
[5]P. Wurfel, T. Trupke, T. Puzzer, E. Schaffer, W. Warta, and S. W. Glunz, J. Appl. Phys. **101**, 123110 (2007).
[6]H. A. Zarem, P. C. Sercel, J. A. Lebens, L. E. Eng, A. Yariv, and K. J. Vahala, Appl. Phys. Lett. **55**, 1647 (1989).
[7]N. M. Haegel, T. J. Mills, M. Talmadge, C. Scandrett, C. L. Frenzen, H. Yoon, C. M. Fetzer, and R. R. King, J. Appl. Phys. **105**, 023711 (2009).
[8]A. Topaz, B. A. West, T. H. Gfroerer, and M. W. Wanlass, Appl. Phys. Lett. **90**, 092110 (2007).
[9]A. T. Hunter, Proc. SPIE **623**, 36 (1986).
[10]W. Shockley and W. T. Read, Jr., Phys. Rev. **87**, 835 (1952); R. N. Hall, ibid. **87**, 387 (1952).